JVSTA Journal of Vacuum Science & Technology A

Etching mechanism of the single-step through-silicon-via dry etch using SF6/C4F8 chemistry

Zihao Ouyang, D. N. Ruzic, Mark Kiehlbauch, Alex Schrinsky, and Kevin Torek

Citation: Journal of Vacuum Science & Technology A **32**, 041306 (2014); doi: 10.1116/1.4885500
View online: http://dx.doi.org/10.1116/1.4885500
View Table of Contents: http://scitation.aip.org/content/avs/journal/jvsta/32/4?ver=pdfcov
Published by the AVS: Science & Technology of Materials, Interfaces, and Processing

Articles you may be interested in

Finite-element simulation models and experimental verification for through-silicon-via etching: Bosch process and single-step etching
J. Vac. Sci. Technol. A **32**, 041303 (2014); 10.1116/1.4882215

Silicon etch using SF6/C4F8/Ar gas mixtures
J. Vac. Sci. Technol. A **32**, 041302 (2014); 10.1116/1.4880800

Fabrication of 3D charged particle trap using through-silicon vias etched by deep reactive ion etching
J. Vac. Sci. Technol. B **31**, 032001 (2013); 10.1116/1.4799662

Low-pressure inductively coupled plasma etching of benzocyclobutene with SF6/O2 plasma chemistry
J. Vac. Sci. Technol. B **30**, 06FF06 (2012); 10.1116/1.4758765

Kinetics of electron attachment to SF3CN, SF3C6F5, and SF3 and mutual neutralization of Ar+ with CN and C6F5
J. Chem. Phys. **134**, 044323 (2011); 10.1063/1.3529423

HIDEN ANALYTICAL
Instruments for Advanced Science

Gas Analysis
- dynamic measurement of reaction gas streams
- catalysis and thermal analysis
- molecular beam studies
- dissolved species probes
- fermentation, environmental and ecological studies

Surface Science
- UHV TPD
- SIMS
- end point detection in ion beam etch
- elemental imaging - surface mapping

Plasma Diagnostics
- plasma source characterization etch and deposition process reaction
- kinetic studies
- analysis of neutral and radical species

Vacuum Analysis
- partial pressure measurement and control of process gases
- reactive sputter process control
- vacuum diagnostics
- vacuum coating process monitoring

Contact Hiden Analytical for further details:
W www.HidenAnalytical.com
E info@hiden.co.uk
CLICK TO VIEW our product catalogue

Redistribution subject to AVS license or copyright; see http://scitation.aip.org/termsconditions. Download to IP: 128.174.163.244 On: Sat, 23 Aug 2014 20:53:39

Etching mechanism of the single-step through-silicon-via dry etch using SF_6/C_4F_8 chemistry

Zihao Ouyang[a] and D. N. Ruzic
Center for Plasma Material Interactions, Department of Nuclear Plasma and Radiological Engineering, University of Illinois at Urbana-Champaign, Urbana, Illinois 61801

Mark Kiehlbauch, Alex Schrinsky, and Kevin Torek
Micron Technology, Inc., 8000 South Federal Way, Boise, Idaho 83707

(Received 25 March 2014; accepted 11 June 2014; published 26 June 2014)

A single-step etching method using the SF_6/C_4F_8 chemistry is developed in this study as an alternative through-silicon-via (TSV) etching approach of the traditional Bosch process to realize ultrasmooth and vertical TSV profiles. Experimental results show that there is a profile discontinuity, or a "transition," on the TSV profile produced by the single-step etching method at high bias voltages and high SF_6 flow rates. Comparison between the intensity of the species generated in a pure SF_6 or a pure C_4F_8 plasma and in a SF_6/C_4F_8 plasma is investigated for better understanding interactions between SF_6 and C_4F_8. The densities of all positive ions are reduced in the SF_6/C_4F_8 plasma compared to a pure SF_6 plasma and a pure C_4F_8 plasma at the same partial pressure, indicating a change of plasma chemistry when SF_6 and C_4F_8 fluxes are mixed. The formation mechanism of the transition is proposed as a chemistry discontinuity caused by large-angle ion sputtering at the top part of the sidewalls and the polymer accumulation at the bottom part of the sidewalls. The formation of the transition has found to have an effect of improving the sidewall smoothness below the position where it is formed. Parameter study has shown that a decreased bias voltage and a reduced SF_6/C_4F_8 ratio can help to improve the sidewall smoothness and eliminate the transition on the TSV profiles. © *2014 American Vacuum Society*. [http://dx.doi.org/10.1116/1.4885500]

I. INTRODUCTION

Through silicon via (TSV) is an important structure in the back end of line applications in current semiconductor industry. TSVs are typically used to interconnect function units of logic and memory chips to realize 3D integration. Appropriate TSV etching technique has the potential to become a critical approach to overcome the scaling limit by obtaining high module density, low operation power and high bandwidth in 3D integrated devices.[1] Typical TSV features have relatively large critical dimensions (CDs) of 1–50 μm and aspect ratios up to 15:1.[2] TSV profiles significantly affect the quality of subsequent filling steps for a "via-first" process, and therefore the overall electrical performance of the stacked chips.

A common approach for TSV structures is to perform an alternating etching and passivation steps, known as the Bosch process.[3] In the Bosch approach, fluorine-rich gases, frequently SF_6, are used as the etch gas to maximize etch rate (ER) during the etching step, and fluorocarbon gases, such as C_4F_8, C_4F_6, and CHF_3 are effective in forming polymers on sidewalls during the passivation step.[3–5] However, an intrinsic problem of the Bosch process is the scalloped TSV profile on the sidewalls. Scalloped profiles are undesirable because they can induce voids and defects in the subsequent metal filling processes, leading to physical and electrical failure on devices.

An alternative approach for TSV etching proposed by Tachi and colleagues in 1988 has shown that sidewall passivation in trench features is possible by mixing CF_4 and $CBrF_3$ gases to a SF_6 plasma when the etch temperature is below $-100\,^{\circ}C$.[6] This type of etch processes is referred as the "cryogenic process." One of the advantages of the cryogenic etch is that it simultaneously controls the etching and passivation balance at both the bottom and sidewalls of TSVs. The cryogenic etch represents a steady-state process, which does not generate scallops on TSV sidewalls due to a continuous etching/passivation chemistry. In most recent cryogenic processes, SF_6 and O_2 are frequently used to obtain an anisotropic etch pattern by effectively passivating sidewalls. In the SF_6/O_2 chemistry, neutral fluorine (F) atoms are believed to be the main etch radicals and the passivation layer is reported to be an oxide-fluoride compound (SiO_xF_y) film with a thickness of 10–20 nm.[7] Cryogenic processes often utilize hard masks to prevent mask cracking at low temperature. Trenches with an ER of $\sim$4 μm/min, an aspect ratio of larger than 10:1, and a silicon/mask selectivity of 750 can be achieved by cryogenic process using SiO_2 hard masks.[8] However, vertical profiles may not be obtained using a steady-state chemistry due to depletion of both ions and etching radicals as feature depth increases, known as the "aspect ratio dependent etching" (ARDE). It is known that the loss mechanism of radicals and ions are different: radical depletion is governed by the Knudsen transport and surface reactions, and ion loss is contributed by scattering and deflection to sidewalls by an initial angular distribution.[9] A common issue of TSV profiles realized by the cryogenic process is the bowing at the top of the feature as a result of the ARDE.[8] On the other hand, the practical limitations of using

[a]Electronic mail: ouyang2@illinois.edu

Redistribution subject to AVS license or copyright; see http://scitation.aip.org/termsconditions. Download to IP: 128.174.163.244 On: Sat, 23 Aug 2014 20:53:39

very low temperature often have production issues in terms of cost and efficiency.

This study explores the feasibility of a near room-temperature single-step process for TSV etching using the SF_6/C_4F_8 chemistry, by investigating the roles of the ion and neutral species in the processing plasma at various experimental conditions. Suggestions on the etching/passivation regime of the single-step TSV etching are therefore provided from the results of this study.

II. EXPERIMENT

Experiments in this study are carried out in the LAM 2300 SyndionC etching system (LAM Research, USA). The LAM2300 SyndionC system is an inductively coupled plasma (ICP) system, as shown in Fig. 1. There are several key advantages of the SyndionC system for TSV etching, including (1) continuously tunable etching parameters, such as chamber pressure, gas flow rate, and bias voltage for various etching process; (2) high top power and bottom bias power; (3) multiple materials, including dielectrics, conducting films, and silicon, can be etched in this tool *in-situ*. Therefore, capital cost and cycle time for TSV etching can be reduced by avoiding the need for multiple etch systems.

A mass spectrometer (Hiden Analytical Ltd., UK) is used in this study to investigate the plasma species at different experimental conditions. The mass spectrometer is essentially an Electrostatic Quadrupole Plasma (EQP) analyzer, which consists of a high-transmission 45° sector field ion energy analyzer and a quadrupole mass spectrometer. The EQP analyzer is capable of recording the energy and mass-to-charge ratio distributions of positive ions, negative ions, and neutral species from a plasma using different operation modes. In this study, the mass spectrometer is calibrated in a SF_6 plasma. SF_5^+ and F^- ions are used to optimize the ion extraction optics and sector energy filter for positive ions and negative ions, respectively.

Industrial standard 300 mm TSV pattern wafers are used throughout this study. A 2 μm hardmask consisting of SiO_2 and Si_3N_4 and a 4.5 μm photoresist reticle are patterned on the TSV wafers, with an 8 μm CD of the TSV feature. The hardmask is opened with a SF_6 and C_4F_8 plasma before TSV etching.

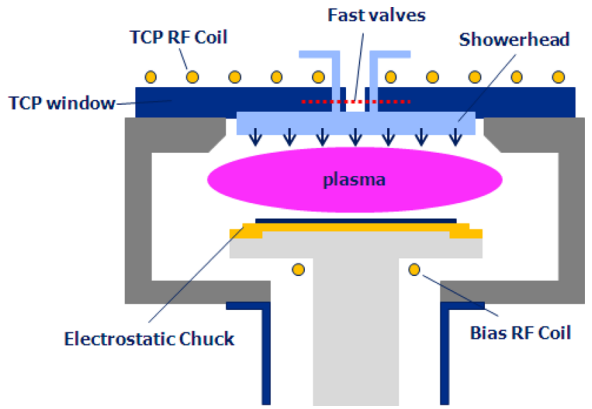

FIG. 1. (Color online) Schematic diagram of the LAM Syndion C system with a transformer coupled plasma (TCP) window.

III. RESULTS AND DISCUSSION

Experimental work performed in this study involves using a mixture of SF_6 and C_4F_8 gases to enable the TSV etching and passivation simultaneously. It is expected that the chemistry in a SF_6/C_4F_8 plasma is much more complicated than that in a pure SF_6 or a pure C_4F_8 plasma due to interactions between species dissociated from SF_6 and C_4F_8. However, it is not fully understood yet what types of chemical reactions would occur when the plasma species from SF_6 and C_4F_8 molecules interact with each other, either by theoretical simulation or experiments. One can speculate that the number density of fluorine species (positive ions, negative ions, and neutral F) can be affected by mixing SF_6 and C_4F_8 gases together in a plasma. The chemical balance of fluorine species created by dissociation of SF_6 molecules can be significantly shifted by interactions with C_xF_y species from C_4F_8 dissociation, as listed in Table I. This mechanism can significantly

TABLE I. Reactions enhanced by F-species (ions and radicals) in a SF_6/C_4F_8 plasma.

Reaction	Rate coefficient ($cm^3\ s^{-1}$)	Reference
$F + CF_3 \rightarrow CF_4$	2.0×10^{-11}	10
$F + CF_2 \rightarrow CF_3$	1.8×10^{-11}	11
$F + CF \rightarrow CF_2$	9.96×10^{-11}	12
$F + C_2F_4 \rightarrow CF_3 + CF_2$	4.8×10^{-11}	13
$F + C_2F_5 \rightarrow CF_3 + CF_3$	1.0×10^{-11}	14
$F + C_3F_6 \rightarrow C_3F_7$	1.0×10^{-12}	14
$F + C_2F_3 \rightarrow C_2F_4$	1.0×10^{-12}	14
$F + CF_3 + M \rightarrow CF_4 + M$	1.6×10^{-28}	13
$F_2 + CF_2 \rightarrow CF_3 + F$	8.3×10^{-14}	12
$F_2 + CF_3 \rightarrow CF_4 + F$	1.9×10^{-14}	15
$F_2 + C_2F_4 \rightarrow C_2F_5 + F$	3.5×10^{-16}	16
$F_2 + C_3F_6 \rightarrow C_3F_7 + F$	3.5×10^{-16}	16
$F^- + CF_3^+ \rightarrow F + CF_3$	8.7×10^{-8}	17
$F^- + CF_2^+ \rightarrow F + CF_2$	9.1×10^{-8}	17
$F^- + CF^+ \rightarrow CF + F$	9.8×10^{-8}	17
$F^- + C_2F_5^+ \rightarrow F + C_2F_5$	9.0×10^{-8}	18 and 19
$F^- + C_2F_3^+ \rightarrow F + C_2F_3$	9.0×10^{-8}	18 and 19
$F^- + CF_3^+ \rightarrow CF_2 + F_2$	8.7×10^{-8}	17
$F^- + CF_3^+ \rightarrow CF_2 + F + F$	3.0×10^{-7}	17
$F^- + CF_2^+ \rightarrow CF + F_2$	9.1×10^{-8}	17
$F^- + C_2F_4^+ \rightarrow CF + CF_2 + F_2$	8.2×10^{-8}	17
$F^- + C_3F_5^+ \rightarrow C_2F_4 + CF_2$	8.0×10^{-8}	17
$F^- + C_3F_6^+ \rightarrow C_2F_4 + CF_3$	8.0×10^{-8}	17
$F^- + C_3F_7^+ \rightarrow C_2F_6 + CF_2$	8.0×10^{-8}	17
$F^- + C_4F_7^+ \rightarrow C_2F_5 + CF_2$	8.0×10^{-8}	17
$F^+ + CF_2 \rightarrow CF^+ + F_2$	2.28×10^{-9}	17
$F^+ + CF_3 \rightarrow CF_2^+ + F_2$	2.90×10^{-9}	17
$F^+ + CF_4 \rightarrow CF_3^+ + F_2$	1.0×10^{-9}	17
$F^+ + C_2F_4 \rightarrow C_2F_3^+ + F_2$	1.0×10^{-9}	17
$F^+ + C_2F_6 \rightarrow C_2F_3^+ + F_2$	1.0×10^{-9}	17
$F^+ + C_2F_5 \rightarrow C_2F_4^+ + F_2$	1.0×10^{-9}	17
$F_2^+ + CF \rightarrow CF_2^+ + F$	2.18×10^{-9}	17
$F_2^+ + CF_2 \rightarrow CF_3^+ + F$	1.79×10^{-9}	17
$F_2^+ + CF_3 \rightarrow CF_3^+ + F + F$	1.60×10^{-9}	17
$F_2^+ + CF_4 \rightarrow CF_3^+ + F + F_2$	1.0×10^{-10}	17
$F_2^+ + C_2F_4 \rightarrow C_2F_4^+ + F_2$	1.0×10^{-10}	17
$F_2^+ + C_2F_5 \rightarrow C_2F_5^+ + F_2$	1.0×10^{-10}	17

Redistribution subject to AVS license or copyright; see http://scitation.aip.org/termsconditions. Download to IP: 128.174.163.244 On: Sat, 23 Aug 2014 20:53:39

reduce the silicon ER due to the loss of fluorine atoms used in etching. The other possible interaction mechanism is that the addition of the SF_6 species can modify the polymerization process and change the chemical composition of the deposited polymer films, compared with a pure C_4F_8 plasma. More importantly, the chemical interactions also depend on variables such as SF_6:C_4F_8 gas mixture ratio, chamber pressure, RF power, and bias voltage.

Comparison between the intensity of the species generated in a pure SF_6 or a pure C_4F_8 plasma and in a SF_6/C_4F_8 plasma can provide important information for understanding the chemical interactions between SF_6 and C_4F_8 in a plasma. The relative intensity of the positive ions and neutrals taken into account in a pure SF_6 and a pure C_4F_8 plasma are shown in Figs. 2 and 3, respectively.

Figure 2 shows the mass spectroscopy data from a pure SF_6 plasma at a RF power of 1500 W and a pressure of 60 mTorr. It is seen that SF_3^+ is the most dominant positive ions in the SF_6 plasma, followed by SF_2^+ (notice that the intensity of SF_3^+ ion is plotted with a different scale). This result disagrees with the simulation data reported in Ref. 20 and the experimental data reported in Ref. 21, in which cases SF_5^+ is found to be the most dominant positive ion species at a power range of 50–3500 W and a pressure range of 30–150 mTorr. This indicates that the ion composition is pushed to a more dissociated state at high RF power. Another possible reason is that the chemical

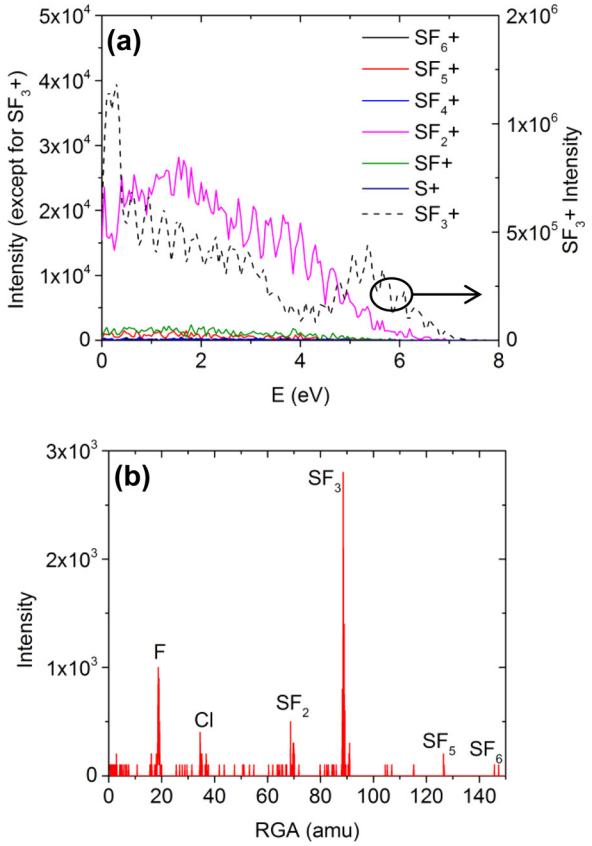

FIG. 2. (Color online) Mass spectroscopy of (a) positive ions and (b) neutral species of a SF_6 plasma at 200 sccm, 1500 W, and 60 mTorr.

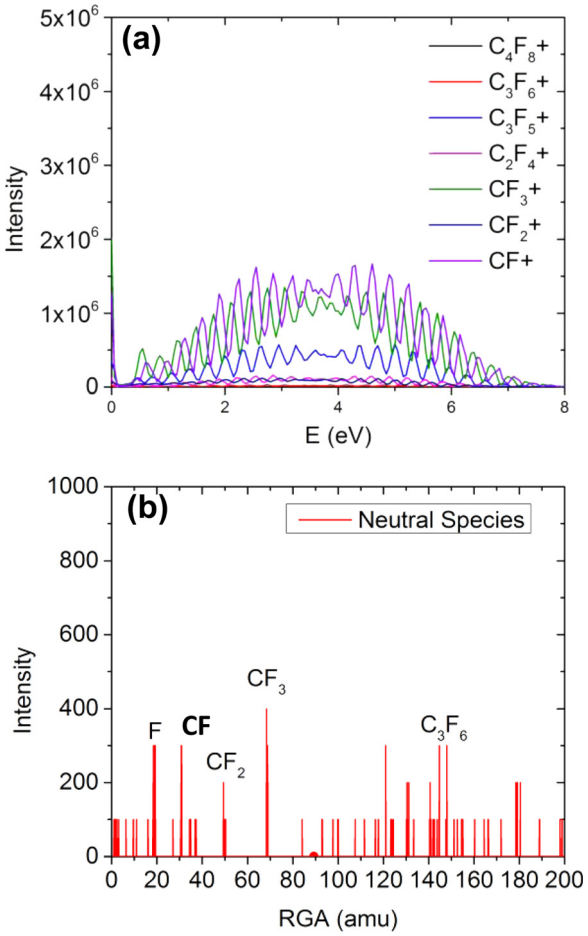

FIG. 3. (Color online) Mass spectroscopy of (a) positive ions and (b) neutral species of a C_4F_8 plasma operated at 200 sccm, 1500 W, and 40 mTorr.

balance of SF_5^+ consumption reactions is enhanced in the plasma so that the rate coefficient for dissociation ionization reaction

$$SF_5^+ + SF_6 \rightarrow SF_3^+ + SF_6 + F_2 \quad (1)$$

becomes dominant at this experimental condition. It can be seen from Fig. 4 that when T_e is less than ~2 eV, the rate coefficient of $SF_6 \rightarrow SF_3^+$ is larger than that of $SF_6 \rightarrow SF_5^+$, and reaction (1) becomes a major reaction for SF_3^+ ion generation. This T_e range is typical for an inductively coupled plasma etcher (such as LAM Syndion C in this study), especially when it is operated at relatively high pressure and low power.

Positive ions and neutral species generated in a pure C_4F_8 plasma at a RF power of 1500 W and a pressure of 40 mTorr are compared in Fig. 3. The sinusoidal pattern in the ion densities in the mass spectroscopy is possibly caused by the digital modulation of the dwell time. It is clear that CF_3^+ and CF^+ are the most dominant positive ions in this case. This observation disagrees with the simulation data reported by Vasenkov *et al.*[22] if the major branching of C_2F_4 dissociation is assumed by

$$C_2F_4 \rightarrow CF_2 + CF_2, \quad (2)$$

Redistribution subject to AVS license or copyright; see http://scitation.aip.org/termsconditions. Download to IP: 128.174.163.244 On: Sat, 23 Aug 2014 20:53:39

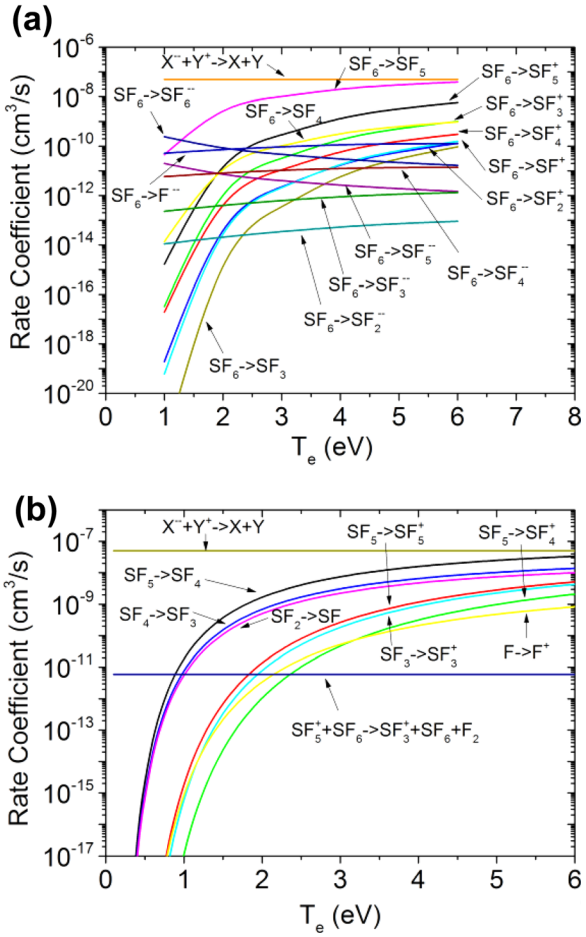

FIG. 4. (Color online) Rate coefficients of the major reactions of the (a) SF_6 ions and molecules and (b) SF_x ($x < 6$) ions and molecules in a SF_6 plasma.

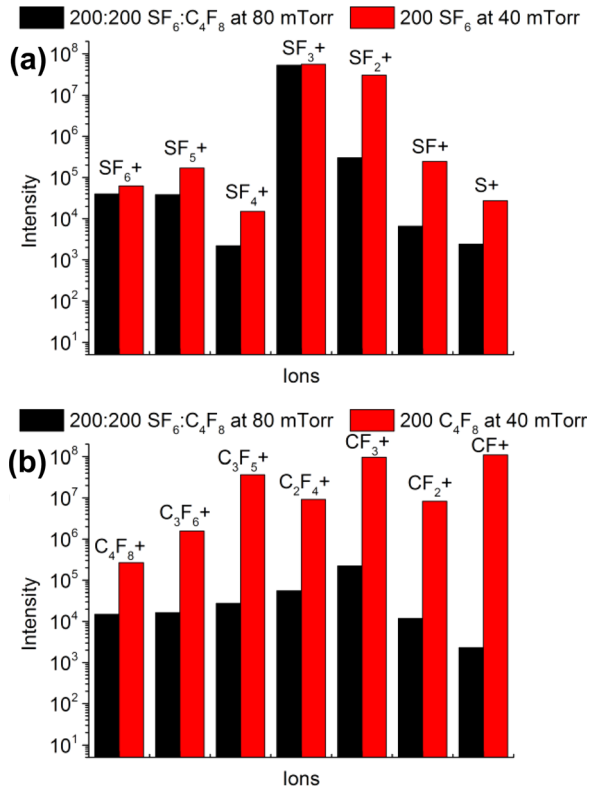

FIG. 5. (Color online) Comparison of the mass spectroscopy data of the positive ions from (a) a pure SF_6 and (b) a pure C_4F_8 plasma and a SF_6/C_4F_8 plasma at a RF power of 1500 W.

in which case CF_2^+ are the dominant positive ions. However, the authors stated that if 50% of C_2F_4 dissociation is assumed to be

$$C_2F_4 \rightarrow CF_3 + CF, \tag{3}$$

the simulation results are in better agreement with experiments. Since CF_2^+ ions are observed as a minor species as shown in Fig. 3(a), it is concluded that the C_2F_4 dissociation by Eq. (3) is the dominant reaction. It is also noticed in Fig. 3(a) that the ion energy distributions (IEDs) of all species consist of two peaks with a small energy separation of ~2 eV. The proposed mechanism for this observation is the difference in threshold energies of C_4F_8 dissociation paths for CF_3^+ generation, either through C_3F_5

$$\begin{aligned} &C_4F_8 \rightarrow CF_3^+ + C_3F_5, \\ &C_4F_8 \rightarrow C_3F_5^+ + CF_3 \rightarrow CF_3^+ + C_3F_5, \end{aligned} \tag{4}$$

or through C_2F_4

$$\begin{aligned} &C_4F_8 \rightarrow C_2F_4^+ + C_2F_4 \rightarrow CF_3^+ + CF + C_2F_4, \\ &C_4F_8 \rightarrow C_2F_4^+ + C_2F_4 \rightarrow C_2F_4^+ + CF_3^+ + CF. \end{aligned} \tag{5}$$

The small separation of two energy peak indicates that the threshold energy of these two dissociation reaction paths is similar. The threshold energies of reactions (4) and (5) are found to be 14.4 eV and 12.35 eV,[23] which agree with the energy peak separation in Fig. 3(a).

The comparisons of the major species from a mixed SF_6/C_4F_8 plasma and from a pure SF_6 or C_4F_8 plasma have been shown in Figs. 5 and 6, respectively. The experimental conditions for a pure SF_6 or C_4F_8 plasma are at a gas flow rate of 200 sccm and at a pressure of 40 mTorr. The SF_6/C_4F_8 plasma is operated with 200 sccm SF_6 and 200 sccm C_4F_8 at a pressure of 80 mTorr so that the plasma has

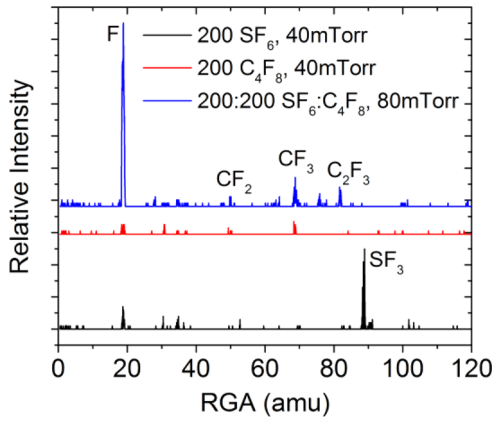

FIG. 6. (Color online) Comparison of the mass spectroscopy data of the neutral species from a pure SF_6 or C_4F_8 plasma and a SF_6/C_4F_8 plasma at a RF power of 1500 W.

Redistribution subject to AVS license or copyright; see http://scitation.aip.org/termsconditions. Download to IP: 128.174.163.244 On: Sat, 23 Aug 2014 20:53:39

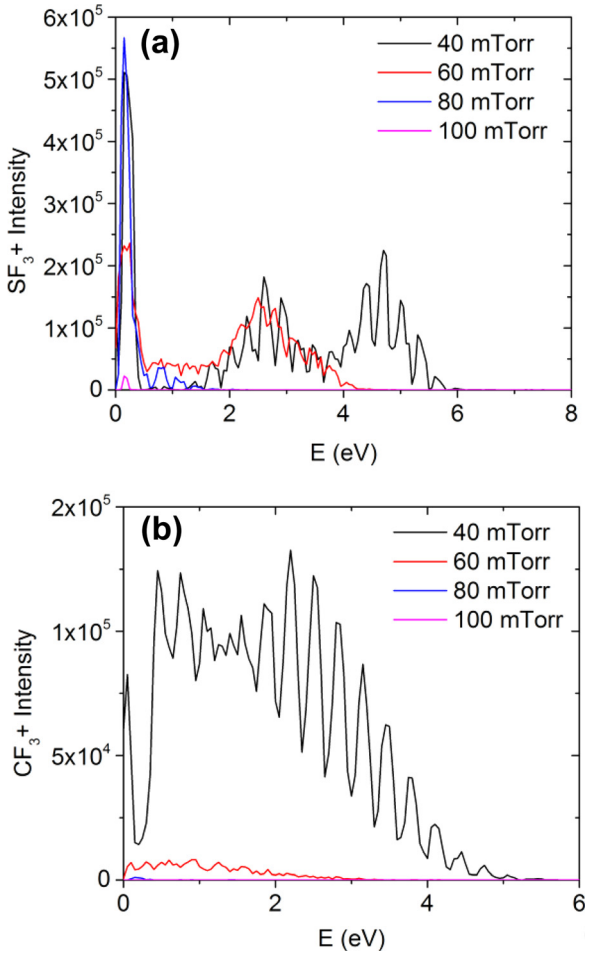

FIG. 7. (Color online) Comparison of the mass spectroscopy data of the intensity of (a) SF_3^+ and (b) CF_3^+ ions of SF_6/C_4F_8 plasmas at different pressures.

the same SF_6 or C_4F_8 partial pressure. It is known that the partial pressure can be expressed as

$$P_{\text{partial}} V_{\text{total}} = P_{\text{total}} V_{\text{partial}}, \tag{6}$$

where P is the pressure and V is the volume. Since the volume is the flow rate times time, the partial pressure is simply depending on the ratio of the partial flow rate over the total flow rate. In this study, the SF_6 and C_4F_8 both have a partial pressure of 40 mTorr in the SF_6/C_4F_8 plasma. However, it is noticed that for electron-impact dissociation, the partial pressure of different ion and neutral species cannot be expressed by Eq. (6) since the electron temperature decreases at an increased pressure.

It can be seen from Fig. 5 that the number densities of all positive ions are reduced in a SF_6/C_4F_8 plasma, compared to a pure SF_6 plasma and a pure C_4F_8 plasma at the same partial pressure. This may result from either a weaker ionization due to the decrease of electron density or a stronger positive–negative ion neutralization when mixing SF_6 and C_4F_8 together. However, it is found that the intensity decrease is much more significant for lighter species, such as SF_2^+, SF^+, S^+, CF_2^+, and CF^+ ions, compared to heavier species, such as SF_6^+, SF_5^+, and $C_4F_8^+$. This observation indicates

TABLE II. Baseline single-step TSV etching process.

RF power (W)	V_{bias} (V)	Pressure (mTorr)	SF_6 (sccm)	C_4F_8 (sccm)	Time (s)
3000	100	80	200	200	600

that the electron-impact ionization is weakened in a SF_6/C_4F_8 plasma, since the lighter ions are mainly created by electron-impact dissociation.

Another observation from Fig. 5 is that the intensity of the SF_3^+ ions in the SF_6/C_4F_8 plasma is only slightly decreased, compared to a pure SF_6 plasma. This again indicates that SF_3^+ ions are generated not only by the electron-impact dissociations from SF_6 but also other multistep dissociations from heavy SF_x species through three-body interactions in a SF_6/C_4F_8 plasma.

The comparison of neutral species of the SF_6/C_4F_8 plasmas and pure SF_6 or C_4F_8 plasmas is shown in Fig. 6. It can be seen that the intensity of the neutral F atoms is much higher in the SF_6/C_4F_8 plasma than the sum of that of the pure SF_6 and C_4F_8 plasmas. However, the intensity of the neutral SF_3 is much lower in the SF_6/C_4F_8 plasma, which may be consumed in producing SF_3^+ ions by electron-impact ionization. Major polymer-forming monomers (C_xF_y neutrals), such as CF_2, CF_3, and C_2F_3, are generally increased in the SF_6/C_4F_8 plasma. This implies that the passivation mechanism would be enhanced if a SF_6/C_4F_8 plasma is used for TSV etching processes.

The IEDs of two of the most dominant positive ions in a SF_6/C_4F_8 plasma, SF_3^+ and CF_3^+, are compared in Fig. 7 at different operating pressures. It can be seen that, at a relatively low pressure (40 mTorr and 60 mTorr), the IED of the SF_3^+ ions consists of a low-energy peak and one or more high-energy peaks, whereas the IED of CF_3^+ ions consists of one or more medium-energy peaks. At an increased pressure (80 mTorr), the energy difference between the SF_3^+ and CF_3^+ ions is reduced. Finally, ions are thermalized at ~0.2 eV when the pressure is further increased to

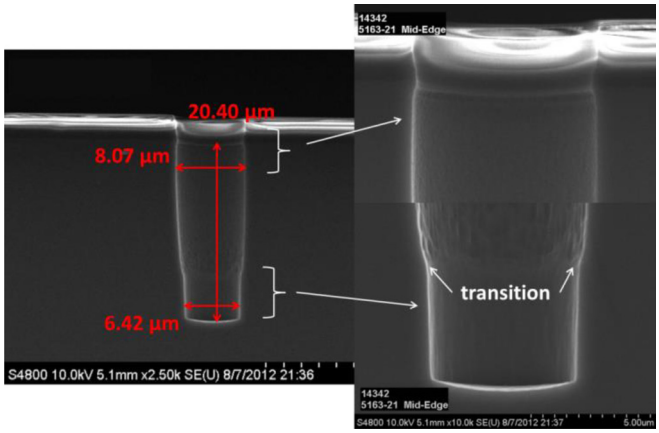

FIG. 8. (Color online) TSV etch profile made by the baseline single-step etching process in Table II. A transition is clearly seen on the TSV sidewalls.

Redistribution subject to AVS license or copyright; see http://scitation.aip.org/termsconditions. Download to IP: 128.174.163.244 On: Sat, 23 Aug 2014 20:53:39

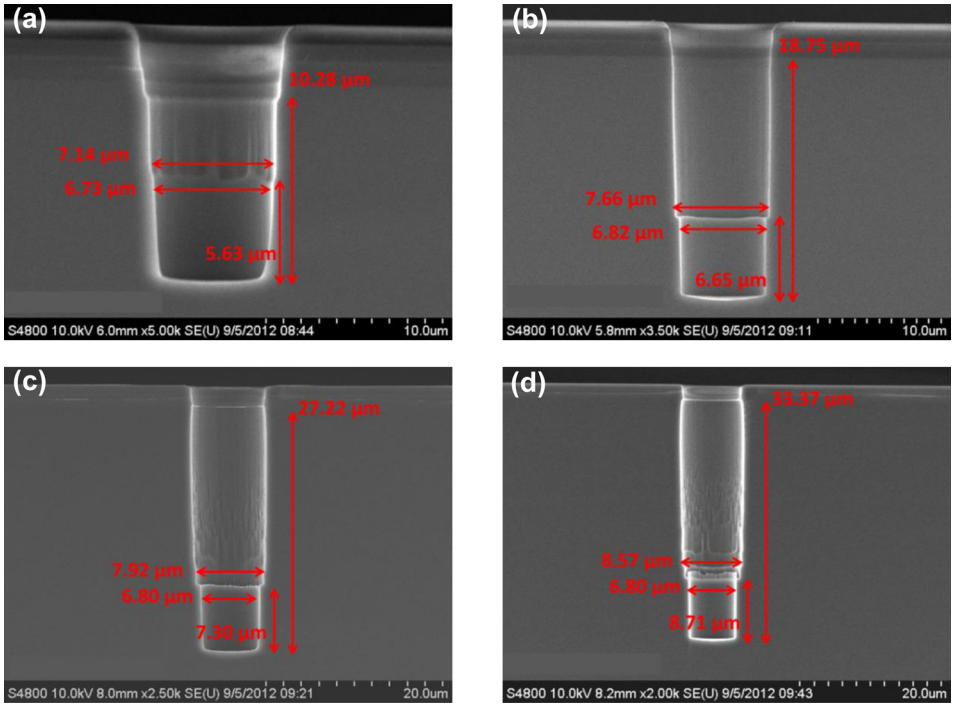

FIG. 9. (Color online) Evolution of TSV profile etched by the single-step etching process in Table III with a total etch time of (a) 100 s, (b) 200 s, (c) 300 s, and (d) 400 s.

100 mTorr. The different behaviors of the IEDs of SF_3^+ and CF_3^+ ions indicate that there is a discrepancy between the ion angular distributions of SF_3^+ and CF_3^+ when they arrive at the substrate surface, especially for a low-pressure etching process. Since CF_3^+ is one of the dominant species in ion-enhanced polymer deposition and SF_3^+ is the dominant polymer sputtering ion species, the different angular distributions of these two ion species can result in polymer removal preferably at some surface locations than others. As a result, the ERs at different surface locations are significantly affected by the ion flux distribution, which eventually determine the etch profile.

Understanding the plasma chemistry in the TSV etching is important for interpreting the etching kinetics at different experimental conditions. It has been shown earlier in this paper that the behavior of almost all the plasma species is distinct in a SF_6/C_4F_8 plasma compared to a pure SF_6 or a pure C_4F_8 plasma. This suggests that if a Bosch process with the optimal etching (SF_6) and passivation (C_4F_8) chemistry balance has been found to realize good anisotropic TSV profiles, the single-step process by mixing the same amount of SF_6 and C_4F_8 gases would not result in an optimized anisotropic TSV etch profile due to the chemistry shift from SF_6/C_4F_8 interactions. The effects of the ions and neutrals in the SF_6 and C_4F_8 will be further explored with experiments in the following paragraphs.

TABLE III. TSV etching process used for etch profile evolution.

RF power (W)	V_b (V)	Pressure (mTorr)	SF_6 (sccm)	C_4F_8 (sccm)
3000	200	80	220	100

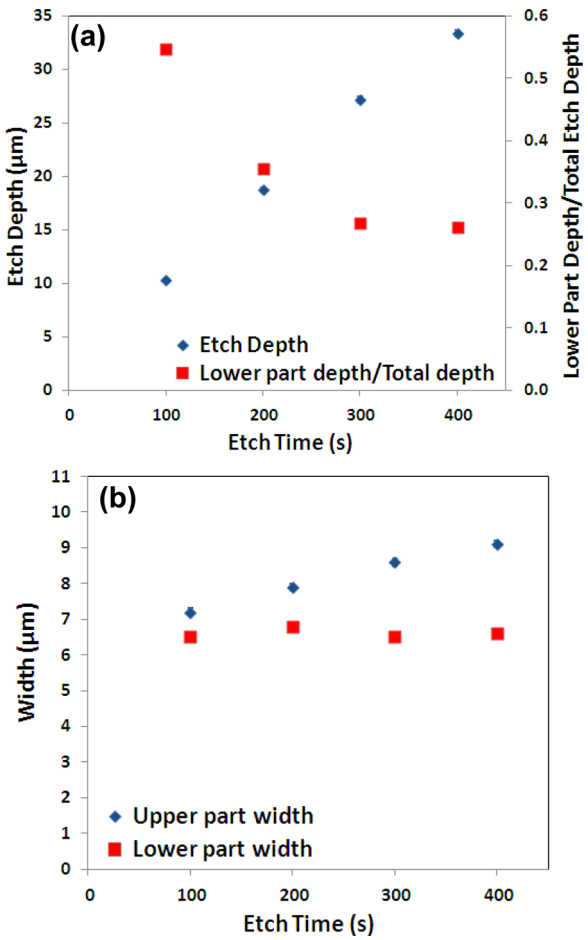

FIG. 10. (Color online) (a) Time dependence of etch depth and lower part/total etch depth ratio. (b) Time dependence of the profile widths of upper and lower part of the TSVs.

Redistribution subject to AVS license or copyright; see http://scitation.aip.org/termsconditions. Download to IP: 128.174.163.244 On: Sat, 23 Aug 2014 20:53:39

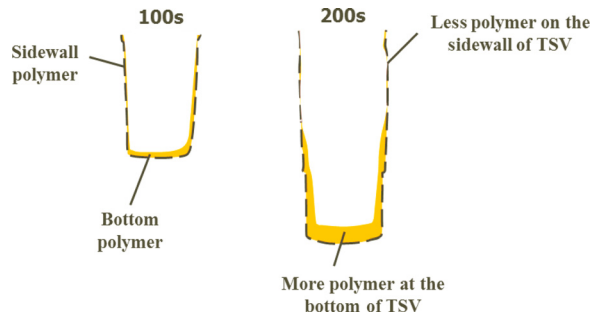

FIG. 11. (Color online) Diagram illustrating the proposed mechanism for transition formation on etch profiles produced by single-step etching.

The baseline single-step TSV etching process using a mixture of SF_6 and C_4F_8 (SF_6:$C_4F_8 = 200$:200) is listed in Table II, and the resulting TSV profile is shown in Fig. 8. It is interesting that a profile discontinuity, or a profile "transition," is found on the sidewalls of the TSV, as a result of this steady-state single-step process. It is noticed that the quality of the top part (above the transition) and the bottom part (below the transition) of the profile have distinct sidewall smoothness. The top part shows striations of up to 0.3 μm in width on the sidewalls, but the bottom part is smooth and no striations are visible.

Detailed study is required in order to appropriately explain the formation of the transition and its evolution as a function of time. More importantly, whether or not the formation of the transition can be controlled by manipulating the process parameters is critical for practical TSV applications of the single-step etching method. In order to investigate the origin of the transition formation, TSV profiles produced at 100–400 s are compared in Fig. 9 using the experimental conditions listed in Table III.

TABLE IV. SF_6 flow rate modification for the baseline single-step TSV etching process at 80 mTorr.

TCP power (W)	V_b (V)	Pressure (mTorr)	SF_6 (sccm)	C_4F_8 (sccm)	Time (s)
3000	100	80	(a) 225 (b) 200 (c) 175	200	600

It can be seen from Fig. 9 that the transition on the TSV sidewalls appears as early as an etching time of 100 s, and it is evolving with the total etch time in both lateral and vertical directions. However, it can be seen that the widths of the bottom part of TSVs do not significantly change with time. These results are compared in Fig. 10.

It can be speculated that the reasons for the sidewall roughness and bowing above the transition are related to the large angular-spread ion bombardment and insufficient passivation at the top of the etch profile, and the IED plays an important role in producing the transition on the TSV profile. The mechanism of the transition formation is therefore proposed and schematically illustrated as Fig. 11: Polymer films deposited on sidewalls at the top of the TSV are governed by neutral (conformal) deposition and can be quickly cleared by polymer sputtering ions, such as SF_3^+, incident at nonvertical angles. On the other hand, polymer deposition on the sidewalls at the bottom of the TSV is not cleared fast enough

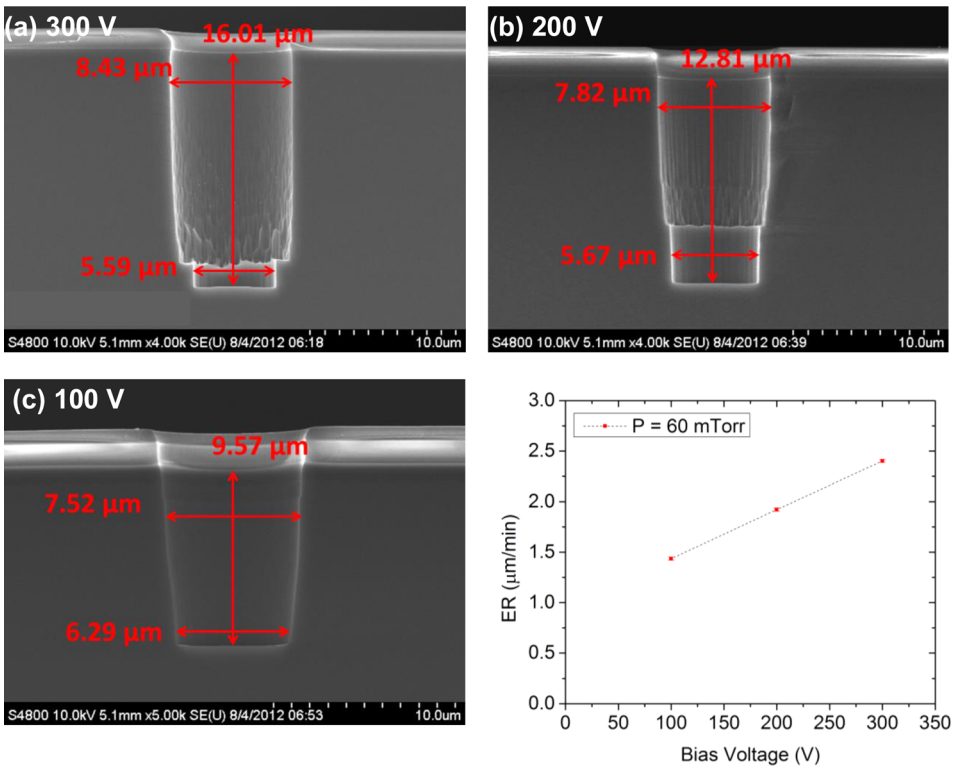

FIG. 12. (Color online) TSV etch profiles obtained by the single-step etching profile with a bias voltage of (a) 300 V, (b) 200 V, and (c) 100 V with etch time of 400 s. ER is compared in (d).

Redistribution subject to AVS license or copyright; see http://scitation.aip.org/termsconditions. Download to IP: 128.174.163.244 On: Sat, 23 Aug 2014 20:53:39

because of the ion-enhanced deposition. Monomers of the ion-enhanced deposition monomers, such as CF_2^+, have a significantly smaller angular distribution than neutral deposition monomers, such as CF_2, leading to polymer accumulation at the bottom of the TSV profiles. As etch depth increases, there is a location with equal contributions of polymer sputtering and deposition forming on the profile sidewalls. The sidewalls above this position are dominated by etching, and the sidewalls below this position are dominated by passivation. This is the origin of the initial transition on the sidewalls. After the transition is formed on the sidewalls [as shown in Fig. 9(a)], it blocks a small portion of ions entered at relatively large angles to prevent them from reaching the sidewalls beyond the transition, resulting in smoother sidewalls below the transition, as seen in Figs. 9(b)–9(d).

In order to verify the proposed mechanism for the transition formation, the effect of the (V_b) is investigated based on the baseline single-step etching process. The TSV profiles produced at 300 V, 200 V, and 100 V at a pressure of 60 mTorr are compared in Fig. 12. It can be seen that the bias voltage plays an important role in the formation of the transition. The transition can be characterized by the CD difference above and below the transition. The CD difference above and below the transition is decreased from 2.8 μm at a bias voltage of 300 V to 2.2 μm at 200 V, and the transition is not observed in the etch profile at a bias voltage of 100 V. Another phenomenon observed in Fig. 12 is that the TSV profile is more vertical when the bias voltage is increased, which indicates a more tightened ion angular distribution is obtained at a higher bias voltage. The increase of the ER as a function of the bias voltage is almost linear, as shown in Fig. 12(d). This is a combined effect of a higher polymer sputtering yield[24] and an increased ion-enhanced Si etching yield.[25] For F-based chemistry, the linearity behavior of ER on the bias voltage can be expressed by

$$\mathrm{ER} \propto \sqrt{E_i}(E_i - 10)^{0.5}, \tag{7}$$

where the ion energy E_i is proportional to the bias voltage. It can be seen from Eq. (7) that if $E_i \gg 10$ eV, ER is linearly depending on the ion energy, or the bias voltage.

Since the bias voltage is an important factor in the transition formation on the TSV profiles, it is reasonable to believe that the determining factor of the TSV morphology is the ions which are affected by the bias voltage. Assuming the transition formation is related to the bombardment of ions from SF_6, directly changing the number density of sputtering ions by increasing or decreasing the SF_6 to C_4F_8 ratio should have an impact for the transition formation as well. The investigation of SF_6 flow rate variation has been performed at a pressure of 80 mTorr and at a bias voltage of 100 V, as shown in Table IV, and the resulting TSV profiles are compared in Fig. 13. It is clear that the transition is easier to form at a higher SF_6 flow rate.

The parametric study of the bias voltage and gas flow shows that the transition formed on the TSV sidewalls using the single-step etching approach is related to the number

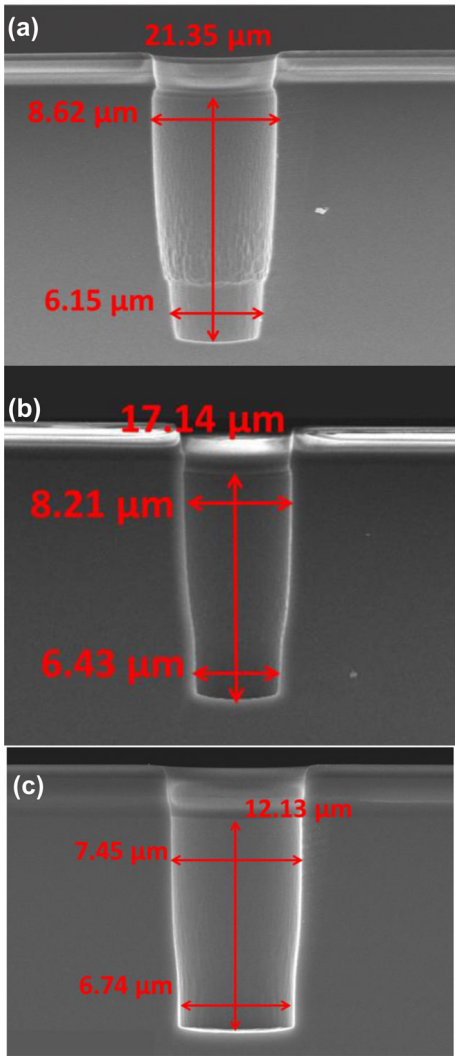

FIG. 13. (Color online) TSV etch profiles obtained by the single-step etching profile with a SF_6 flow rate of (a) 225 sccm, (b) 200 sccm, and (c) 175 sccm at 80 mTorr.

density of ions and ion angular distribution. Since the transition is most likely not desirable in the TSV profiles due to the fact that the discontinuity of the TSV can cause electrical failure after metal filling, selecting appropriate combinations of bias voltage and gas flows can provide solutions of eliminating the transition and obtaining a smooth TSV profile. Several candidates for transition-free single-step TSV processes are listed in Table V and the resulting TSV profiles are shown in Fig. 14. It can be seen that the approaches for reducing the transition are reducing the bias voltage, or/and

TABLE V. Modified single-step TSV etching processes in order to achieve transition-free TSV profiles.

RF power (W)	V_b (V)	Pressure (mTorr)	SF_6 (sccm)	C_4F_8 (sccm)	Time (s)
(a) 3000	100	60	225	200	600
(b) 3000	100	80	200	200	600
(c) 3000	100	100	175	200	600
(d) 3000	80	80	200	200	600

Redistribution subject to AVS license or copyright; see http://scitation.aip.org/termsconditions. Download to IP: 128.174.163.244 On: Sat, 23 Aug 2014 20:53:39

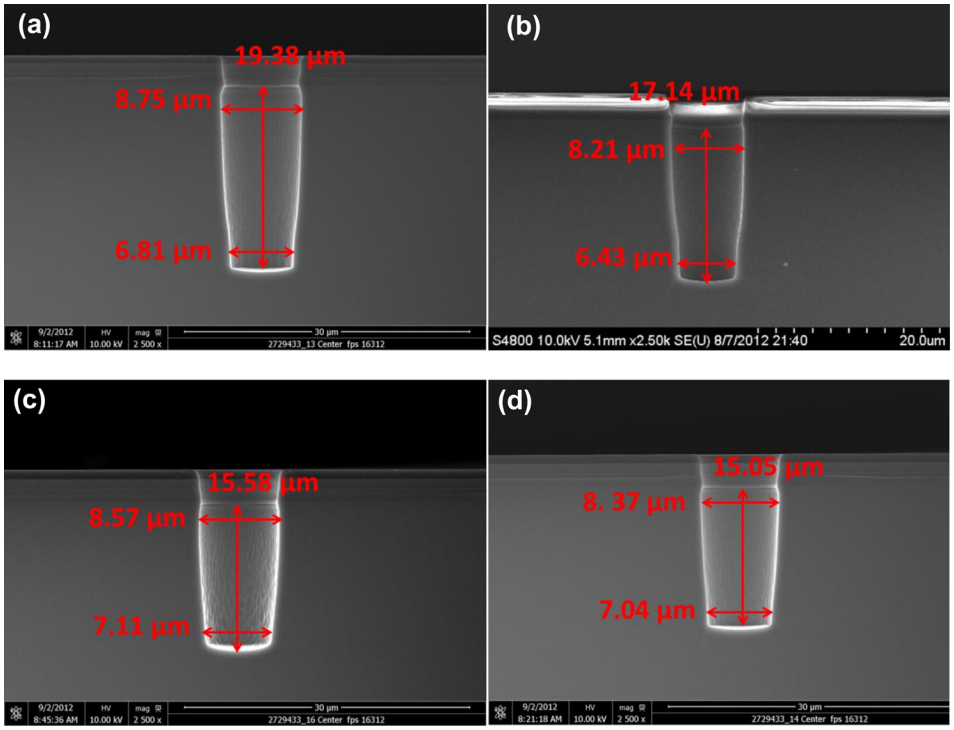

FIG. 14. (Color online) TSV profile etched by the single-step etching processes in Table V at different pressure, bias voltage, and SF_6 flow rate combinations.

decreasing the SF_6 flow rate. Sidewall smoothness can be improved by reducing the pressure, or/and decreasing the SF_6 flow rate.

It can be seen from Fig. 14 that the single-step etching processes in Table V effectively eliminate the visible transition on the TSV profile at a pressure of 60 and 80 mTorr, and improve the profile smoothness at 100 mTorr. It is noticed that a discontinuity is about to appear on the sidewalls in Figs. 14(a) and 14(b), which is characterized by a drastic CD decrease from the top to the bottom of the etch profiles. On the other hand, TSV profiles produced by process (c) and (d) have more continuous sidewalls. TSV etched by process (d) has smaller top bowing and more smooth sidewalls compared to process (c), which makes it a suitable candidate for producing TSVs using the single-step etching method.

IV. CONCLUSION

The mechanisms for the single-step TSV etching using the SF_6/C_4F_8 chemistry have been studied by investigating the plasma chemistry and varying process parameters. It is found that the balance between the etching and passivation chemistry are shifted due to the interactions of the dissociated species from SF_6 and C_4F_8, compared to a pure SF_6 etching chemistry, or a pure C_4F_8 passivation in the traditional Bosch process.

An observation of the TSV profiles realized by the single-step etching processes is the transition discontinuity formed on the sidewalls. The mechanism of the transition formation is found to be significantly affected by the bias voltage, pressure and SF_6 flow rate. However, the direct cause of the transition is proposed in this study as a synergistic mechanism of large-angle ion bombardment at the top sidewalls of the etch profile and the polymer accumulation at the bottom sidewalls. This mechanism results in a discrepancy in the surface roughness above and below the transition. It is found that the transition is evolved from a small discontinuity on the etch profile and will further grow deeper and wider into a distinct step due to preferable etching in the vertical direction.

It is concluded from experimental results that decreasing bias voltage, reducing SF_6 flow rate, and increasing pressure can prevent the transition from forming at an early stage. A common result of all these three approaches is to reduce the density of the high-energy etching ions from SF_6. As a result, each of these approaches will lead to a low ER, and a large sidewall roughness on etch profiles.

The single-step etching method for producing TSV profiles is capable of etching scallop-free profiles and has low requirements on the etching system. However, its complexity inherited in the methodology of combining the etching and passivation chemistries will possibly result in a small process window for a production-worthy process because this method has control on the physical and chemical process of individual plasma species compared to the Bosch process.

ACKNOWLEDGMENTS

This work was supported by Micron Technology, Inc. The authors would like to thank the dry etch group for great support and discussion.

[1]J. Burns, L. McIlrath, C. Keast, C. Lewis, A. Loomis, K. Warner, and P. Wyatt, "Three-dimensional integrated circuits for low-power, high-bandwidth systems on a chip," *IEEE International Solid-State Circuits Conference, Digest of Technical Papers* (2001), pp. 268–269.
[2]B. Wu, A. Kumar, and S. Pamarthy, J. Appl. Phys. **108**, 051101 (2010).

Redistribution subject to AVS license or copyright; see http://scitation.aip.org/termsconditions. Download to IP: 128.174.163.244 On: Sat, 23 Aug 2014 20:53:39

[3]F. Laermer and A. Schilp, "Plasma polymerizing temporary etch stop," U.S. patent 5501893 A, (26 March 1996).
[4]H. Rhee, H. Kwon, C. K. Kim, H. J. Kim, J. Yoo, and Y. W. Kim, J. Vac. Sci. Technol., B **26**, 576 (2008).
[5]A. A. Ayón, R. Braff, C. C. Lin, H. H. Sawin, and M. A. Schmidt, J. Electrochem. Soc. **146**, 339 (1999).
[6]S. Tachi, K. Tsujimoto, and S. Okudaira, Appl. Phys. Lett. **52**, 616 (1988).
[7]M. J. Walker, Proc. SPIE **4407**, 89 (2001).
[8]M. W. Pruessner, W. S. Rabinovich, T. H. Stivater, D. Park, and J. W. Baldwin, J. Vac. Sci. Technol., B **25**, 21 (2007).
[9]M. A. Blauw, T. Zijlstra, R. A. Bakker, and E. van der Drift, J. Vac. Sci. Technol., B **18**, 3453 (2000).
[10]I. C. Plumb and K. R. Ryan, Plasma Chem. Plasma Process. **9**, 409 (1989).
[11]C. Tsai, S. M. Belanger, J. T. Kim, J. R. Lord, and D. L. McFadden, J. Phys. Chem. **93**, 1916 (1989).
[12]D. R. Burgess, M. R. Zachariah, W. Tsang, and P. R. Westmoreland, Prog. Energy Combust. Sci. **21**, 453 (1995).
[13]N. I. Butkovskaya, M. N. Larichev, I. O. Leipunskii, I. I. Morozov, and V. L. Talroze, Kinet. Katal. **21**, 263 (1980).
[14]K. R. Ryan and I. C. Plumb, Plasma Chem. Plasma Process. **6**, 231 (1986).
[15]E. L. Keating and R. A. Matula, J. Chem. Phys. **66**, 1237 (1977).
[16]V. L. Orkin and A. M. Chaikin, Kinet. Katal. **23**, 438 (1982).
[17]G. I. Font, W. L. Morgan, and G. Mennenga, J. Appl. Phys. **91**, 3530 (2002).
[18]J. T. Moseley, R. E. Olson, and J. R. Peterson, Case Stud. At. Phys. **5**, 1 (1975).
[19]A. P. Hickman, J. Chem. Phys. **70**, 4872 (1979).
[20]G. Kokkoris, A. Panagiotopoulos, A. Goodyear, M. Cooke, and E. Gogolides, J. Phys. D: Appl. Phys. **42**, 055209 (2009).
[21]R. Foest, J. K. Olthoff, R. J. VanBrunt, E. C. Benck, and J. R. Roberts, Phys. Rev. E **54** 1876 (1996).
[22]A. V. Vasenkov, X. Li, G. S. Oehrlein, and M. J. Kushner, J. Vac. Sci. Technol., A **22**, 511(2004).
[23]C. Lifshitz and R. Grajower, Int. J. Mass Spectrom. Ion Phys. **10**, 25 (1972/1973).
[24]S. Rauf, W. Dauksher, S. Clemens, and K. Smith, J. Vac. Sci. Technol., A **20**, 1177 (2002).
[25]C. Steinbruchel, Appl. Phys. Lett. **55**, 1960 (1989).

Redistribution subject to AVS license or copyright; see http://scitation.aip.org/termsconditions. Download to IP: 128.174.163.244 On: Sat, 23 Aug 2014 20:53:39